Warping Functions Design for Long Warped ZT-DFT-s-OFDM

Mostafa Ibrahim

Department of Engineering Technology
Texas A&M University
Texas, USA
mostafa.ibrahim@tamu.edu

Sabit Ekin

Departments of Engineering Technology, and Electrical & Computer Engineering Texas A&M University Texas, USA sabitekin@tamu.edu Ali Riza Ekti

Oak Ridge National Laboratory

Tennessee, USA

ektia@ornl.gov

Abstract—Time-frequency warped waveform is a novel type of well-contained waveform composed of raised cosine (RC) pulses with roll-off factors profile customized for spectrally efficient signal containment. The waveform is suited for massive machine-type communication (mMTC), and Internet-of-Things (IoT) applications. The paper is a follow-up to the original work of time-frequency warped waveforms; here, we are proposing a warping function suited for length-independent symbols, which is missing from the previous work. The paper proposes the design steps starting from a piecewise warping function with parts of straight segments and other curved parts. A maximum Out-ofband leakage is used as a criterion to determine the warping function parameters. The roll-off factors profile determined in the previous study is used as a minimum bound for the leakage limits. Gains are presented over Windowed Zero-tail Discrete Fourier Transform-spread-Orthogonal Frequency Division Multiplexing (ZT-DFT-s-OFDM) in the simulations section.

Index Terms—6G and Beyond, Waveform, Time-Frequency Warping, massive machine-type communication, mMTC, IoT.

I. INTRODUCTION

The number of Internet of Things (IoT) connected devices is expected to increaese exponentially in the next decade, serving various use cases with highly diverse requirements. Machine Type Communication (MTC), with its massive and low latency unlimited wireless connectivity, is a key driver in this expanding trend. To support this massive MTC (mMTC) vision, it is required to design ultra-low power receivers, highly efficient sleep modes, and ultra-low-cost MTC devices [1]. This paper uses the concept of time-frequency warping as a waveform modifier on signals intended for relaxed synchronization, energy efficiency, and low latency scenarios [2], [3].

This paper is a follow-up to [3] that proposes a method to create a spectrally efficient, well-contained symbol in time and frequency domains. The idea is to use high roll-off factors for the raised-cosine (RC) shaped pulses near the edges of the symbol and low roll-off factors for the inner pulses. This is because, in a zero-tail DFT-s-OFDM-like symbol, the outer pulses contribute more to the time domain zero tails than the internal pulses. A similar idea was proposed in [4], but without the warping modifier. This high containment enhances the performance in the presence of time dispersion or time and frequency offsets because the power leaked from the edge symbols would be minimal in the time domain. Then,

the pulse occupancy in the frequency domain is controlled by introducing time-axis warping, which will align the spectral occupancy of all the pulses in the frequency domain. As a result, intersymbol interference (ISI) in the time and frequency domains is reduced. The time-frequency warping modifier is used in the fields of signal analysis and wavelet theory. In [5], Evangelista extends the definition of dyadic wavelets to include frequency-warped wavelets. Moreover, the time-frequency plane's flexible orthogonal and non-orthogonal tilings were defined using frequency-warped wavelets. In [6], designing warped variable filters is proposed to fit the frequency response of a signal.

Our previous work in [3] proposed methods to determine an optimized roll-off factors α profile, followed by warping function determination that fits the decided α profile. The paper also proposed a computationally efficient method for the transmitter scheme that splits the modulated waveform into two parts: a middle part with a linear time progression and an edges part with a warped time function. There was, however, no warping function design procedure proposed for this modified split modulation.

This paper proposes a method to define the warping function first because it decides the different block sizes of the transmitter, and then the roll-off factors of the pulses are determined accordingly, which is the opposite order of our previous study. Moreover, the containment utility function, which is used to determine the roll-off factors, will take into consideration the sampling quantization in time. Finally, the containment, as the zero-tails and OOBE power, is compared with a more generic waveform, Windowed ZT-DFT-s-OFDM.

The base symbol that we will use is Zero Tail DFT spread OFDM (ZT-DFT-s-OFDM) [7]; a variation of the (DFT-s-OFDM) modulation, aiming to decrease the zero tails power. DFT-s-OFDM is used as the modulation scheme for Long-Term Evolution (LTE) uplink schemes because of its low peak-to-average power ratio (PAPR), making it suitable for low-power systems.

The rest of this paper is organized as follows; the timefrequency warping theory is discussed in Section II. The piecewise warping function is proposed in Section III. Roll-off factors profile determination is discussed in Section IV. Finally,

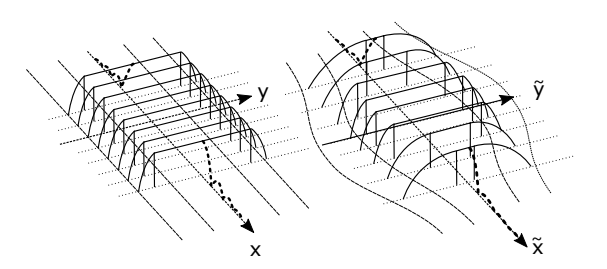


Fig. 1. Windowing versus Axis Warping with gradually changing roll-off factors.

an evaluation of the time-frequency waveform and comparison with the Windowed ZT-DFT-s-OFDM waveforms is provided in Section V.

II. BACKGROUND

In this section, axis warping unitary theory is briefly presented, and its effect is described when applied to the timefrequency plane.

A. Axis Warping Theory

Axis warping transformation is a subclass of unitary transformations. The unitary operator \mathbf{U} is a linear transformation that maps between two Hilbert spaces (i.e., $\mathbf{U}: \mathbf{L}^2(\mathbb{R}) \longmapsto \mathbf{L}^2(\mathbb{R})$). Unitary transformations have the following characteristics. They maintain inner products (i.e., $\langle \mathbf{U}s, \mathbf{U}h \rangle = \langle s, h \rangle$), and they preserve energy (i.e., $\|\mathbf{U}s\|^2 = \|s\|^2$). Axis warping is applied through the warping function w that maps the axis x to the new axis w(x):

$$w: \mathbb{R} \mapsto \mathbb{R}, \quad x \mapsto w(x) ,$$
 (1)

where w is a one-to-one, monotonic function. The warped orthogonal axes \tilde{x} , and \tilde{y} are related to the original axes x and y through:

$$\tilde{x} = w(x), \quad \tilde{y} = y \ \dot{m}(w(x)), \quad (2)$$

where $m = w^{-1}$ is the inverse function of w. Axis warping of waveform s is expressed as follows [8]:

$$[\mathbf{U}s](x) = |\dot{w}(x)|^{1/2} s[w(x)] , \qquad (3)$$

where \dot{w} represents the first derivative of the function w. The warping transform allows for non-uniform axes manipulation and provides a flexible method for controlling time-frequency occupancy.

Time axis warping for an SC-OFDM-based waveform uses axis warping to dilate the time domain pulses at the symbol edges to equalize the effect of the pulses having higher roll-off factors at the symbol edges. The warping concept is shown in Fig. 1 and its comparison with windowing in a generic x-y plane, where x and y can be used to represent time or frequency interchangeably.

In the case of waveform windowing, the shape of the pulse is similar for all pulses. The spacing between the pulses on the x-axis is uniform, and the occupancy in the frequency domain is similar for all of them. On the symbol's edges, the pulse shape has higher roll-off factors and lower tails on the

x-axis for the warped waveform. The pulses with higher rolloff factors have higher occupancy on the y-axis. Therefore, warping is used to shrink the x-y plane on the y-dimension by dilating the x-dimension at the position of the high α pulse. The warping function has to be designed to fit the roll-off factors of the pulses, and the roll-off factors should be chosen to have low power of tails without losing spectral efficiency.

B. Frequency Domain Deformation

Axis warping in the time domain creates deformation in the frequency domain [9]. Let H(f) be the frequency domain response of the unwarped version of the studied waveform. The frequency domain warping deformation results from the operator:

$$\mathbf{W_t} = \mathbf{FWF}^{\dagger},\tag{4}$$

where **F**, and **F**[†] are the Fourier and inverse Fourier transforms, respectively. **W** is warping operator such that; $[\mathbf{W}h](t) = \sqrt{\dot{w}(t)}h[w(t)]$. The first part of the **W**_t operator is

$$\mathbf{W}\mathbf{F}^{\dagger}(t,f) = \int_{\mathbb{R}} \sqrt{\dot{w}(t)} \delta(w(t) - \tau) e^{j2\pi f \tau} d\tau$$

$$= \sqrt{\dot{w}(t)} e^{j2\pi f w(t)}.$$
(5)

Then.

$$\mathbf{FWF}^{\dagger}(f,\nu) = \int_{\mathbb{R}} \sqrt{\dot{w}(t)} e^{j2\pi\nu w(t)} e^{-j2\pi f t} dt.$$
 (6)

So, the new shape of H after warping is found by

$$[\mathbf{FWF}^{\dagger}H](f) = \int_{\mathbb{R}} H(\nu) \int_{\mathbb{R}} \sqrt{\dot{w}(t)} e^{-j2\pi(ft - \nu w(t))} dt d\nu.$$
(7)

The output of this operation can not be found analytically for warped RC pulses or windows [10]. Therefore in the following sections, numerical methods will be used to calculate the frequency domain leakage based on the previous formulation.

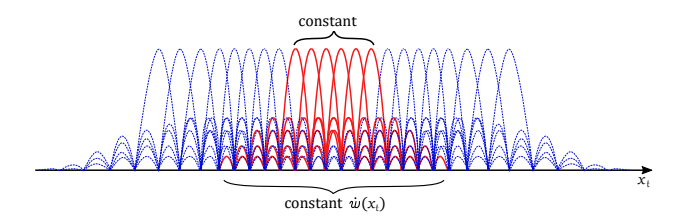


Fig. 2. Splitting modulation regions for lower computational complexity.

C. Split Transmitter Scheme

This section revisits the Split transmitter scheme proposed in [3]. Filter banks are the straightforward choice, given the varying roll-off factors of the pulses, but they come at the expense of computational complexity. Our previous paper introduced an efficient computational complexity method for the transmitter and receiver, which forms the basis of our current work. To reduce complexity in the transmitter filter bank, we consider the $\dot{w}(x_t)$ function with a flat middle. For symbols with a high number of pulses, the middle region

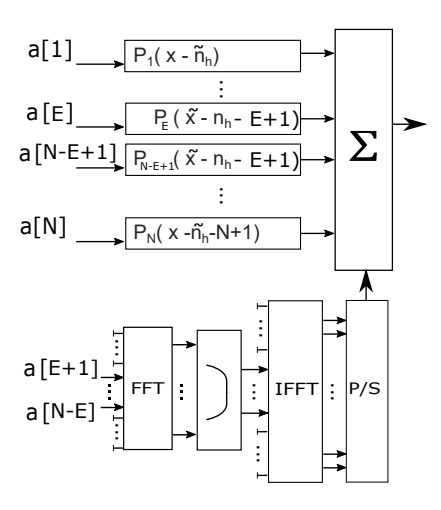


Fig. 3. Splitting modulation regions transmitter scheme.

has a constant α value. This allows for a warping function with a consistent slope over this pulse region, taking into consideration the duration of the effect of these pulses on the time axis.

Fig. 2 illustrates the middle pulses (solid red line) and the edge pulses (blue dotted line). The constant $\dot{w}(x_t)$ region extends to include the middle pulses and their tails, with the duration dependent on the minimum α value. Since the middle pulses are not warped, they can be modulated by a parallel structure of the DFT-s-OFDM modulator, as shown in Fig. 3. The DFT-s-OFDM section includes a long IFFT output to match the sampling rate of the filter bank section responsible for the warped pulses.

The proposed modulation region split reduces computational complexity by utilizing efficient FFT and IFFT blocks. Additionally, the IFFT block can be more efficient through pruning, which excludes VN - 2N inputs from the IFFT butterfly structure.

III. WARPING AND ROLL-OFF FACTOR PROFILES DESIGN

In the previous study, the warping function followed a sigmoid profile, which does not suit the structure of the split modulation scheme. In this section, we propose a warping function specifically designed for this scheme, aiming to minimize the number of parameters for optimization and be more fitting to the scheme.

A. Piecewise Warping Function Design

The warping function, depicted in Fig. 4, consists of straight segments with constant slopes in the middle and at the ends, connected by curved segments. Fig. 4 illustrates the warping function from the center pulse position to one of the edges, and the function exhibits odd symmetry around the center pulse.

The warping function can be mathematically formulated as follows:

$$w(x_t) = \begin{cases} \frac{x_t}{V} & ; |x_t| < w^{-1}(E1) \\ \frac{x_t}{2V} + sign(x_t) \left(\frac{N}{2} - \frac{k}{2}\right) & ; |x_t| > w^{-1}(E2) , \\ ax_t^3 + bx_t^2 + cx_t + d & ; Otherwise, \end{cases}$$
(8)

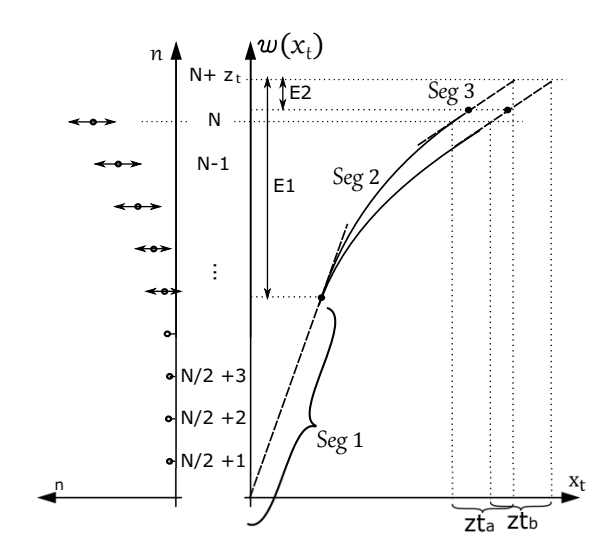


Fig. 4. Warping function determination.

where E1 and E2 are the points in the warped domain where the segments are connected, k represents the extension in pulse widths, and (a, b, c, d) are variables controlling the cubic spline.

To avoid interpulse interference caused by peaks and zeros falling between sampling points, the sampled warping function at the sampling instances $(w(x_t) ; x_t \in \mathbb{Z})$ should have integer values at the sampling points $w^{-1}(n)$. Consequently, in the implementation, the curved segments (Seg 2) within the interval $w^{-1}(E1) < |x_t| < w^{-1}(E2)$ are divided into spline subsegments that connect between the anchor points $(w^{-1}(n), n)$ closest to Seg 2.

We have three main parameters that control the shape of the warping function E1, E2, and k. Segment Seg 1, covering the inner pulses with low roll-off factors, corresponds to the interval $|x_t| < w^{-1}(E1)$ and has a slope of 1/V, where V represents the oversampling ratio. The edge segment Seg 3 has half the slope because we designed the symbol to cover the full roll-off factors range. The zero tails fall within the region of Seg 3.

The extension factor k determines the extent to which the warped pulse is stretched in the time domain. Fig. 4 displays two examples with the same E1 and E2 parameters but different k values. A higher k value shifts the region of zero tails z_{t_h} to a larger x_t value. Seg 2 has distinct (a, b, c, d)values to connect between Seg 1 and Seg 3 in both cases.

B. Roll-off Factors versus Leakage Profiles

The selection of warping function slopes ensures that pulses at the edges have $\alpha = 1$, while inner pulses have $\alpha \to 0$. The time domain representation of the warped RC pulse is given

The warping function can be mathematically formulated as follows:
$$w(x_t) = \begin{cases} \frac{x_t}{V} & ; |x_t| < w^{-1}(E1) \\ \frac{x_t}{2V} + sign(x_t)\left(\frac{N}{2} - \frac{k}{2}\right) & ; |x_t| > w^{-1}(E2) , \\ ax_t^3 + bx_t^2 + cx_t + d & ; Otherwise, \end{cases}$$

$$RC(t) = \begin{cases} \frac{\pi}{4} \operatorname{sinc}\left(\frac{1}{2\alpha}\right), & ; w(x_t) = \pm \frac{1}{2\alpha} \\ \operatorname{sinc}(w(x_t)) \frac{\cos\left(\frac{1}{2\alpha}\right)}{1 - (2\alpha \ w(x_t))^2} & ; \text{ otherwise,} \end{cases}$$

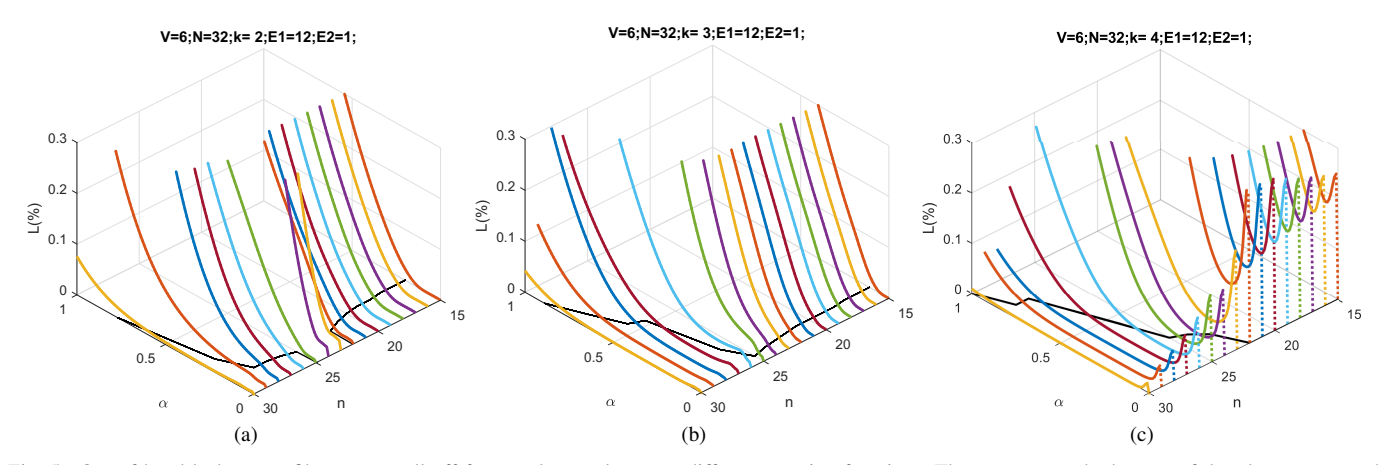


Fig. 5. Out-of-band leakage profiles versus roll-off factors along pulses n at different warping functions. The contours at the bottom of the plots correspond to a leakage value of 0.02%

and the frequency domain representation $\mathbb{RC}(f)$ is formulated as:

$$\mathbb{RC}(f) = \int_{\mathbb{R}} R(\nu) \int_{\mathbb{R}} \sqrt{\dot{w}(t)} \ e^{-j2\pi(ft - \nu w(t))} \ dt \ d\nu \ , \quad (10)$$

where

$$R(\nu) = \begin{cases} 1 & ; \ |\nu| \le \frac{1-\alpha}{2} \\ \frac{1}{2} \left(1 + \cos(\frac{\pi}{\alpha}[|\nu| - \frac{1-\alpha}{2}])\right) & ; \ \frac{1-\alpha}{2} < |\nu| \le \frac{1+\alpha}{2} \\ 0 & ; \ \text{otherwise}. \end{cases}$$
(11)

The frequency domain representation is equivalent to the convolution between the unwarped frequency domain window and the chirp function modulated by $w(x_t)$, as shown in Eq. (10). Since the chirp function exhibits more occupancy and leakage in the frequency domain [10], the convolution result will have some leakage outside the expected spectrum. In this section, we establish limits on the roll-off factors based on the per-pulse leakage function $L_n(\alpha)$. These limits are determined by selecting a maximum leakage value outside a specific band.

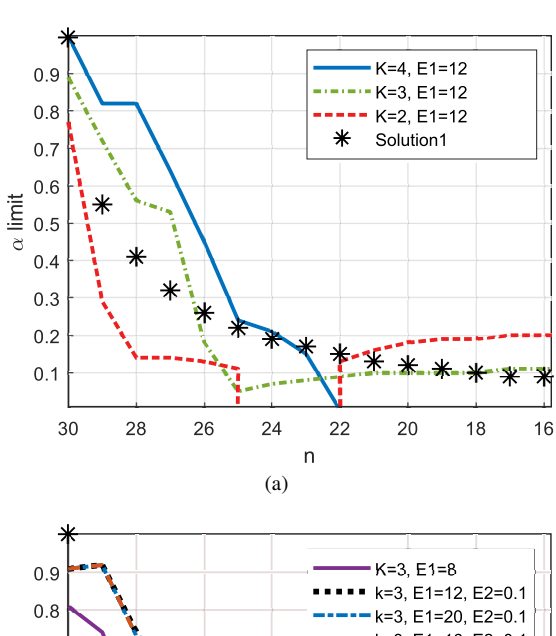
The power leakage ratio \mathbb{L} outside the range $[-f_m, f_m]$ is defined as:

$$\mathbb{L}_n(\alpha) = 1 - \frac{\int_{-fm}^{fm} |\mathbb{RC}_n(f, \alpha)|^2 df}{\int_{-\infty}^{\infty} |\mathbb{RC}_n(f, \alpha)|^2 df}.$$
 (12)

To provide flexibility in the design problem, we allow the band f_m to be higher than the band of the sinc pulse by a factor of ζ , resulting in $f_m = \frac{\zeta f_s}{2V}$. Later, we will demonstrate that the factor ζ is crucial, as without it $(f_m = \frac{f_s}{2V})$, we would not find a solution to unite all pulses under the same spectral mask unless high leakage is allowed.

In Fig. 5, we plot the profile $\mathbb{L}_n(\alpha)$ for k values of 1, 2, and 3, while fixing E1=12, E2=1, and V=6. Additionally, we draw the contour of $\mathbb{L}_n(\alpha)=0.02\%$ to represent the boundaries for selecting α values. In other words, roll-off factors below this boundary are acceptable for the chosen frequency domain leakage.

We can observe different leakage behavior for different k extension values. For a low value of k=2, pulses at



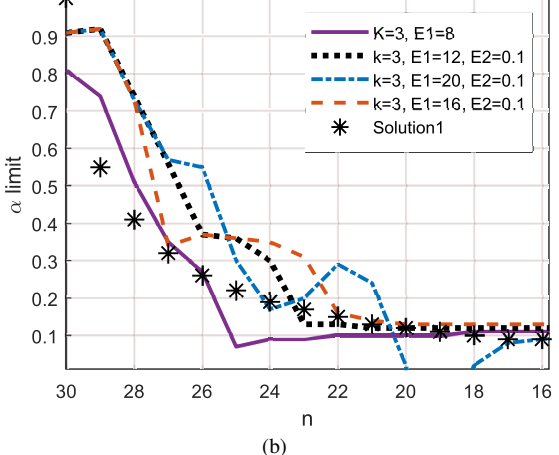


Fig. 6. Roll-off factor boundaries with 0.02 % leakage limits.

the edges and in the middle exhibit a low leakage profile. However, pulses at the transition or curved part of the warped function have a higher leakage profile. On the other hand, for a higher k=3 value, pulses at the edges have low leakage profiles, while inner pulses suffer from high leakage profiles. Interestingly, there exists a near-optimal k value in the middle where the transition is smooth enough for pulses in the curved region yet short enough for the inner pulses. The contours of $\mathbb{L}n(\alpha) = 0.02\%$ are shown in Fig. 6a, along with the rolloff factors profile labeled as "solution 1" from the paper [3]. This roll-off factor profile is determined by solving a marginal utility problem, assuming a cost of $c_n=\frac{1}{1+\alpha_n}$ and a utility gain represented by the power suppression over the first side lobe in the tails region. The roll-off factor profile values for 20 pulses from the edges are as follows: $\rho N \to N - 19 = [1.0]$ 0.55 0.41 0.32 0.26 0.22 0.19 0.17 0.15 0.13 0.12 0.11 0.1 0.09 0.09 0.08 0.08 0.07 0.07 0.06].

For the three contours in Fig. 6a, the closest boundary that fits with the roll-off factor profile is at k=3. By fixing k and further tuning the parameters E1 and E2, we obtain the contours in Fig. 6b. From the figure, we observe that the closest contour to the roll-off profile is achieved at E1=12 and E1=16. However, for E1=8 and E1=20, some pulses in the range $n=[17,\ 26]$ fall below the roll-off factor profile limit ρ due to high leakage.

C. Optimization Solutions

In this section, we discuss two different optimization problems to find the warping function parameters. Linear programming is used to get the maximum spectral efficiency with the minimum out-of-spectrum leakage [11].

First, we formulate an optimization problem that minimizes the product of excess time and excess bandwidth, denoted as η :

$$\eta = \zeta \left(\frac{2k+N}{N} \right). \tag{13}$$

This finds the values of E1, E2, and k that yield an α_n contour with the lowest loss of spectral efficiency while satisfying ρ_n for all n.

$$\min_{E1,E2,k,\zeta} \zeta\left(\frac{2k+N}{N}\right)$$
s.t.
$$\lim_{\alpha_n \to \rho_n} \mathbb{L}_n(\alpha) > L_{min} \quad \forall n,$$
(14)

where L_{min} represents the minimum allowed leakage value. Different solutions can be obtained for different L_{min} values. As the problem inherently allows a range of E1 values, we select the minimum E1 values to minimize computational complexity by reducing the number of filter bank branches.

Table 1 presents the results of Eq. 14 for various leakage tolerance L_{min} values, along with the corresponding $(E1,E2,k,\zeta,\eta)$ values. The optimization is performed for different N values, resulting in different η values, where the subscript denotes the value of N. The solution $(E1,E2,k,\zeta)$ remains the same and is independent of the N values.

TABLE I SOLUTIONS FOR Eq. (14) FOR different L_{min} values, N values and at V=6

	L_{min} $\times 10^{-2}\%$	E1	E2	k	ζ	η_{64}	η_{128}	η_{256}
	0.7	19	0	$\frac{29}{6}$	1.034	1.19	1.112	1.073
İ	1	13	0	š	1.06	1.16	1.109	1.085
İ	3	10	0	2.5	1.046	1.128	1.087	1.066
	5	8	1	3	1.031	1.128	1.079	1.055

The presence of the ζ value in the optimizable parameter η and the boundaries set by \mathbb{L}_n may lead to overly stringent solutions, as will be demonstrated in Section IV. Therefore, we explore an alternative optimization parameter. We consider minimizing the total leakage outside f_m while allowing more tolerance for the ζ value to exceed the expected spectral expansion of the inner pulses. This is formulated as:

$$\min_{E1,E2,k} \quad \sum_{n=1,\cdot,N} \int_{f_m}^{\infty} \mathbb{L}_n(\alpha)$$
s.t. $\zeta = (1 + \alpha_{inner}),$ (15)

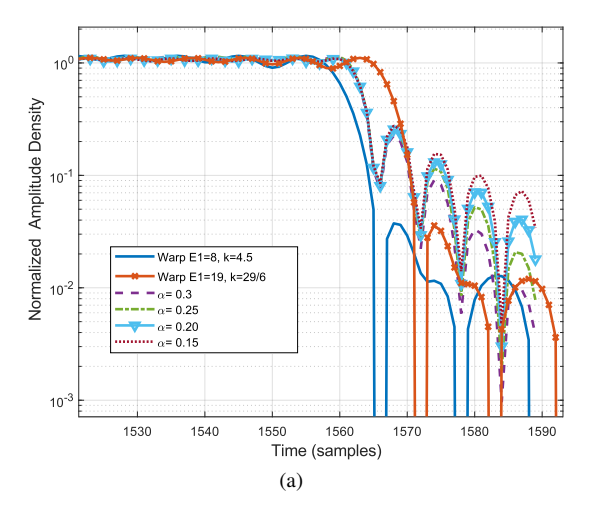
where α_{inner} represents the roll-off factor value of the inner pulses. The solution to this optimization problem will be discussed in the following section and compared with the previous problem.

IV. RESULTS & DISCUSSION

This section presents results comparing the containment of warped waveforms with RC windowed ZT-DFT-s-OFDM, which exhibits lower zero tail power compared to ZT-DFT-s-OFDM. Windowing leads to an expansion in bandwidth. Hence, we compare with different α RC windowing values. It's important to note that this paper does not include a bit-error-rate (BER) performance comparison as it tends to be scenario-specific. In other words, the BER performance gains depend on factors such as separation and power imbalances between similar modulated words in adjacent bands and time slots [3]. On the other hand, containment comparison is more generic and agnostic to interference scenarios.

Previously, we demonstrated that the solution to Eq. (14) yielded the lowest leakage at (E1=19,E2=0,k=29/6). Now, by solving Eq. (15), we obtain the results (E1=8,E2=0,k=4.5) at V=6 and $\zeta=(1+0.1)$. The two solutions are also compared with each other using windowing evaluations in Fig. 7. All symbols have a length of N=251, and the number of zeros for the windowed ZT-DFT-s-OFDM is zt=zh=4, while for the warped symbol, it is zt=zh=2. This ensures that all symbols have approximately the same zero gap. The size of the ZT-DFT-s-OFDM FFT block is $[(251+8)\times 2]$, and the IFFT block is 1589. The RC windowing operation is applied after the FFT block, with different α values for comparison purposes.

We observe the difference between the two warping functions in the frequency domain, Fig. 7b. The result of the optimization Eq. (14) has a steeper drop of around 0.08fs compared to the warping function resulting from Eq. (15). This is due to a more conservative ζ for the first solution. However,



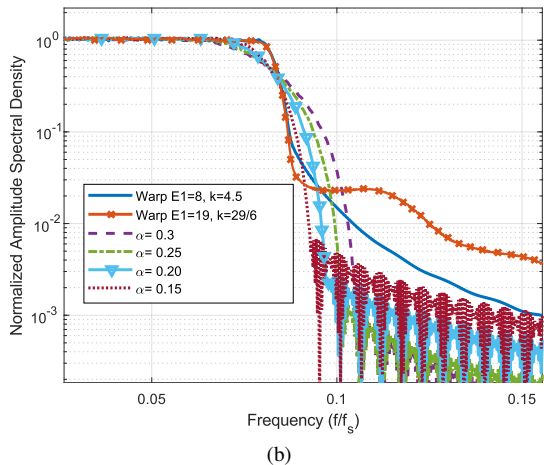


Fig. 7. Time and frequency amplitude densities comparing windowed and warped ZT-DFT-s-OFDM.

this comes at the expense of higher out-of-band leakage after 0.1 fs. The second solution, on the other hand, focuses on minimizing total leakage. Therefore, we prefer the solution obtained from Eq. (15), especially considering that the spectral and temporal occupancy of both solutions are nearly identical.

The RC windowed ZT-DFT-s-OFDM, defined as $\mathbb{F}^{\dagger}(R(f).\mathbb{F}([z_h\ a\ z_t]))$, is simulated with roll-off factors: $\alpha=[0.15,\ 0.2,\ 0.25,\ 0.3]$. For all these cases, it is observed that the zero tails of the warped symbol have lower power in the time domain with reduced spectral occupancy. However, there is an out-of-band leakage that reaches the same level of the windowed symbols after $f=0.15f_s$.

Lastly, the optimization solutions presented in this paper are independent of the symbol length (N value). Additionally, it is found that a minimum leakage solution can be achieved with E2=0. This means that the warping function can be simplified to one straight segment with a slope of $\frac{1}{V}$ in the middle, along with two curved splines at the edges, where the outer end of the curved segment has a slope of $\frac{1}{2V}$.

V. CONCLUSION

This study presents the design and optimization of the warping function for split modulation schemes. A piecewise

warping function was proposed, consisting of straight segments with constant slopes and curved segments to connect them. The shape of the warping function was controlled by parameters such as E1, E2, and k, which determined the roll-off factors and spectral containment. Linear programming optimization was employed to find the optimal values for these parameters, considering factors like spectral efficiency, leakage, and tolerance for spectral expansion. The results demonstrated that different parameter combinations led to varying leakage profiles and spectral occupancy. The optimization solutions were shown to be independent of the symbol length, allowing for a simplified warping function design with fewer parameters.

ACKNOWLEDGMENT

This material is based upon work supported in part by the U.S. Department of Energy, Office of Science, Office of Advanced Scientific Computing Research under Award Number DE-SC0023957. This work was supported in part by the U.S. National Science Foundation under Grants 2323300.

This manuscript has been authored in part by UT-Battelle, LLC, under contract DE-AC05-00OR22725 with the US Department of Energy (DOE). The US government retains and the publisher, by accepting the article for publication, acknowledges that the US government retains a nonexclusive, paid-up, irrevocable, worldwide license to publish or reproduce the published form of this manuscript or allow others to do so for US government purposes. DOE will provide public access to these results of federally sponsored research in accordance with the DOE Public Access Plan (http://energy.gov/downloads/doe-public-access-plan).

REFERENCES

- A. F. Demir, M. Elkourdi, M. Ibrahim, and H. Arslan, "Waveform design for 5G and Beyond," arXiv preprint arXiv:1902.05999, 2019.
- [2] M. Ibrahim, A. F. Demir, and H. Arslan, "Time-Frequency Warped Waveforms," *IEEE Communications Letters*, vol. 23, no. 1, pp. 36–39, 2019.
- [3] M. Ibrahim, H. Arslan, H. A. Cirpan, and S. Ekin, "Time-Frequency Warped Waveforms for Well-Contained Massive Machine Type Communications," *IEEE Journal on Selected Areas in Communications*, pp. 1–1, 2023.
- [4] M. Ibrahim and H. Arslan, "Zero Tail Filter Bank Spread OFDM," in MILCOM 2016 - 2016 IEEE Military Communications Conference, 2016, pp. 688–693.
- [5] G. Evangelista and S. Cavaliere, "Discrete frequency warped wavelets: theory and applications," *IEEE Transactions on Signal Processing*, vol. 46, no. 4, pp. 874–885, 1998.
- [6] Y. Chen, T. Ma, and Y. Wei, "A Design of Variable Digital Filters Based on FRM Technique and Frequency Warping," in 2018 IEEE 23rd International Conference on Digital Signal Processing (DSP), 2018, pp. 1–5.
- [7] G. Berardinelli, F. M. L. Tavares, T. B. Sørensen, P. Mogensen, and K. Pajukoski, "On the Potential of Zero-Tail DFT-Spread-OFDM in 5G Networks," in 2014 IEEE 80th Vehicular Technology Conference (VTC2014-Fall), 2014, pp. 1–6.
- [8] R. G. Baraniuk and D. L. Jones, "Unitary equivalence: a new twist on signal processing," *IEEE Transactions on Signal Processing*, vol. 43, no. 10, pp. 2269–2282, 1995.
- [9] S. Caporale, "Design and Computation of Warped Time-Frequency Transforms," 2009.
- [10] C. Cook, Radar signals: An introduction to theory and application. Elsevier. 2012.
- [11] V. Chvatal, V. Chvatal et al., Linear programming. Macmillan, 1983.